Development of Organic/Inorganic Compatible and Sustainably Bioactive Composites for Effective Bone Regeneration

Nannan Shao,[†,‡] Jinshan Guo,[§] Yuyao Guan,[∥] HuanHuan Zhang,[†] Xiaoyuan Li,[†] Xuesi Chen,[⊥] Dongfang Zhou,*,[†] and Yubin Huang*,[†]

[†]State Key Laboratory of Polymer Physics and Chemistry, Changchun Institute of Applied Chemistry, Chinese Academy of Sciences, Changchun 130022, P. R. China

[‡]University of Science and Technology of China, Hefei 230026, P. R. China

[§]Department of Biomedical Engineering, Pennsylvania State University, University Park, Pennsylvania 16802, United States

[∥]Department of Radiology, China Japan Union Hospital, Jilin University, Changchun 130022, P. R. China

[⊥]Key Laboratory of Polymer Ecomaterials, Changchun Institute of Applied Chemistry, Chinese Academy of Sciences, Changchun 130022, P. R. China

Ⓢ *Supporting Information*

ABSTRACT: In this paper, we demonstrate a strategy of covalently bonding bioactive molecules onto inorganic hydroxyapatite (HAp) to improve the compatibility between organic and inorganic components and endow the bone composites with sustainable bioactivity. Bone morphogenetic protein-2 (BMP-2) peptide covalently immobilized nano-hydroxyapatite (nHAp-BMP-2) is developed to preserve the bioactivity and slow the release of the BMP-2 peptide. Then nHAp-BMP-2 was further incorporated into an ultraviolet-curable mixture of gelatin methacrylamide (GelMA) and four-armed PEG methacrylamide (four-armed PEGMA) to form a Gel/(nHAp-BMP-2) composite. The hydrogen bonding between gelatin and BMP-2 on nHAp-BMP-2 enhanced the compatibility between inorganic and organic components. The Gel/(nHAp-BMP-2) composite exhibited superior biocompatibility caused by gelatin and nHAp-BMP-2, except in a two-dimensional cell culture, the hydrogel was also capable of a three-dimensional cell culture. In addition, the introduction of nHAp-BMP-2 had a positive influence on bone marrow mesenchymal stem cell proliferation, differentiation, and the subsequent calcification on the composite. After treatment of a rat calvarial defect model for 12 weeks, the Gel/(nHAp-BMP-2) group showed the largest new bone volume and the highest ratio of new bone (50.54 ± 13.51 mm^3 and $64.38 \pm 17.22\%$, respectively) compared to those of the other groups. These results demonstrate that this way of controlling BMP-2 release is effective and the Gel/(nHAp-BMP-2) composite has great potential in bone regeneration therapy.
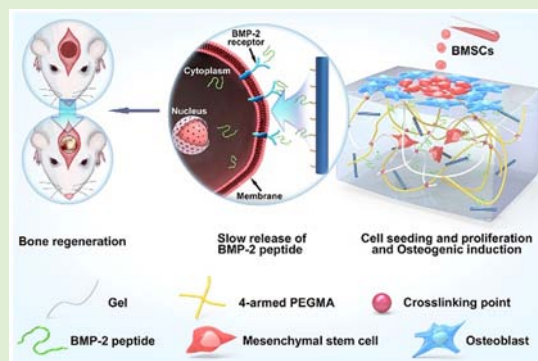
1. INTRODUCTION

Heavy impact, tumor resection, and bone loss all can cause bone injury;[1,2] these actions contribute to approximately 800000 surgical procedures every year, and the number is rapidly increasing with the growth of the aging population.[3] Because of the limited availability, postoperative infection and hemorrhage of an autograft, immune rejection, and the epidemic spreading risks of allografts and xenografts, natural bone grafts are unable to meet the clinical demand.[4] Hence, an increasing number of synthetic bone grafts, with some containing bone-producing stem cells or/and growth factors, have been developed to achieve the curative effect of autologous bone grafts without causing serious side effects.[5] Although promising, synthetic bone grafts,[6−9] especially injectable bone grafts, always suffer from poor organic and inorganic compatibility.[10,11] On one hand, the mechanical strength needs to be improved to meet the application requirement.[12−14] On the other hand, as a "biomaterial", the synthetic bone grafts not only need to fulfill the requirement of the "material" to be physically stable but also need to fulfill the "bio" requirements to be biodegradable, biocompatible, and bioactive so that they can promote cell attachment, proliferation, migration, and nutrient transportation and gradually degrade or be absorbed during tissue regeneration.[15−17]
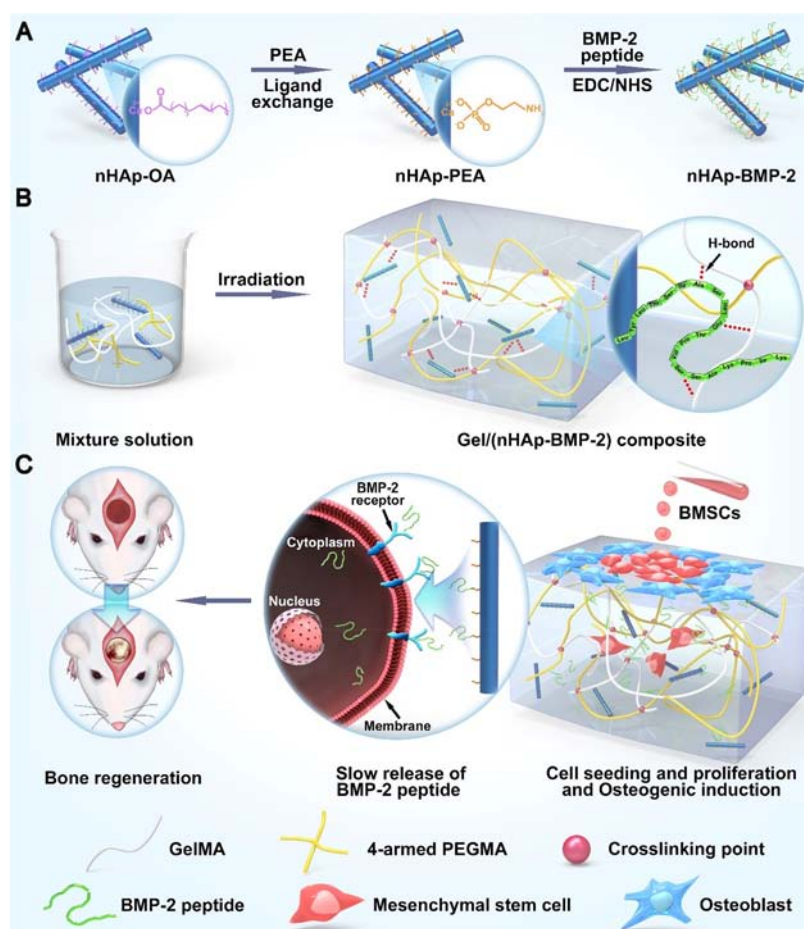
As the main component of connective tissues, the mineralized extracellular matrix (ECM) produced by osteoblasts makes up most of the dry weight of bone.[18−20] In mineralized ECM, type I collagen is one major organic ingredient.[21,22] As a cheap and safe denatured collagen, gelatin

Scheme 1. Illustration of the BMP-2 Peptide Covalently Immobilized Nano-Hydroxyapatite (nHAp-BMP-2)/Gelatin Composite for Effective Bone Regeneration[a]

[a](A) Preparation of nHAp-BMP-2. (B) Fabrication of the Gel/(nHAp-BMP-2) composite by *in situ* photo-cross-linking of GelMA and four-armed PEGMA. (C) *In vitro* and *in vivo* potential of the Gel/(nHAp-BMP-2) composite for effective bone regeneration by slowing the release of the BMP-2 peptide.

is widely available and has been extensively used in biomimetic hydrogel studies because of its close resemblance to natural ECM.[23−25] To mimic the chemical composition of natural bone, some biomimetic inorganic particles, such as hydrox-yapatite (HAp),[26−28] silicate,[29,30] a manganese-doped biore-sorbable ceramic scaffold,[31] and a titanium compound,[32−34] are commonly applied within hydrogels. This leads to an unmet challenge of increasing the organic/inorganic compat-ibility. Meanwhile, to confer the composite hydrogel with improved osteoconduction and osteoinduction activity, various osteogenic growth factors, such as bone morphogenetic proteins (BMPs), transforming growth factors β (TGF-β), platelet-derived growth factor (PDGF), insulin-like growth factor (IGF), etc., have also been loaded within bone grafts.[35] In particular, bone morphogenetic protein 2 (BMP-2), one of the most prominent osteoinductive growth factors used in the clinic,[36] has the impressive ability to stimulate bone marrow mesenchymal stem cells (BMSCs) to differentiate into an osteogenic lineage and ultimately promote bone regeneration in defects.[37−39] However, BMP-2 is apt to be degraded by proteases and has a short lifetime *in vivo*.[40] Burst release of BMP-2 is associated with a series of side effects, such as tissue edema, ectopic bone formation, immunological reaction, and even tumorigenesis.[41−43] Hence, the development of a strategy

for preserving the bioactivity and controlling the release of BMP-2 molecules from the hydrogel is urgently needed.

Here, to improve the compatibility between organic and inorganic components and endow the bone composites with sustainable bioactivity, the BMP-2 peptide (with an amino acid sequence of KIPKASSVPTELSAISTLYL by reference to BMP-2 residues[44,45]) was covalently immobilized onto a nano-hydroxyapatite (nHAp) surface to give nHAp-BMP-2. The nHAp-BMP-2 was then combined with gelatin hydrogel formed by *in situ* photo-cross-linking of gelatin methacrylamide (GelMA) and four-armed PEG_{10K} methacrylamide (four-armed PEGMA) (Scheme 1 and Scheme S1). Because of the slow release of BMP-2 peptides on nHAp-BMP-2, the Gel/(nHAp-BMP-2) composite was endowed with sustainable bioactivity. The combination of BMP-2 and nano-hydrox-yapatite not only preserved the bioactivity of peptides but also avoided allergic reactions caused by burst release. The strong hydrogen bonding between the BMP-2 peptide on nHAp-BMP-2 and GelMA also improved the organic/inorganic compatibility and endowed the composite hydrogel with good mechanical strength. BMSCs were used as a cell model to investigate the biocompatibility and osteoinductive activity of the Gel/(nHAp-BMP-2) composite. To further confirm the effect of the Gel/(nHAp-BMP-2) composite *in vivo*, the

regeneration of skull bone treated by this hydrogel was also studied in rats.

2. EXPERIMENTAL SECTION

2.1. Materials. Octadecylamine, sodium oleate, *O*-phosphoryle-thanolamine (PEA), 1-ethyl-3-[3-(dimethylamino)propyl]-carbodiimide (EDC, 97%), *N*-hydroxysuccinimide (NHS, 98%), gelatin from porcine skin (type A, gel strength of ∼300 g Bloom), methacrylic anhydride (94%), methanesulfonyl chloride (99.7%), Alizarin Red S (ARS), *β*-glycerol phosphate disodium salt (98%), dexamethasone (97%), and Hoechst 33258 (98%) were purchased from Sigma-Aldrich Trading Co., Ltd. (Shanghai, China). Four-armed PEG$_{10K}$-OH (four-armed PEG, 97%) and 2-hydroxy-4′-(2-hydrox-yethoxy)-2-methylpropiophenone (Irgacure 2959, 98%) were obtained from Innochem Co., Ltd. (Beijing, China). BMP-2 peptide (KIPKASSVPTELSAISTLYL sequence, 95.6%) and FITC-labeled BMP-2 peptide (95.6%) were synthesized by Chinapeptides Co., Ltd. (Shanghai, China). The alkaline phosphatase assay kit (Beyotime Institute of Biotechnology), the Pierce BCA protein assay kit (Thermo Fisher Scientific), cell counting kit-8 (CCK-8, Dojindo), Alexa Flour 568 phalloidin (Thermo Fisher Scientific), Calcein AM, propidium iodide (KeyGEN BioTECH), the goldner trichrome stain kit (Solarbio), and all other materials were used as received.

2.2. Characterization. ^{1}H NMR spectra were recorded on a Bruker AV 400 NMR spectrometer at room temperature. Fourier transform infrared (FT-IR) spectra were recorded on a Bruker Vertex 70 spectrometer. The element contents of the hydrogel were identified by X-ray photoelectron spectroscopy (XPS) (Thermo ESCALAB 250). The morphology of nanoparticles was observed by transmission electron microscopy (TEM) using a JEOL JEM-1011 electron microscope. Ultraviolet−visible (UV−vis) spectra were recorded on a Varian Cary 300 UV−vis spectrophotometer using cuvettes with a 1 cm path length, and the standard curve of FITC-BMP-2 was generated. Fluorescent images of nanoparticles and images of live and dead stained BMSCs were taken with a microscope (Nikon TE2000U). The elastic modulus of hydrogels was measured on an AR2000 rheometer (TA Instruments) using a parallel plate (plate diameter of 25 mm, gap of 1 mm) in oscillatory mode at 37 °C. Briefly, the sample was placed on the plate of the rheometer, and the temperature was increased to 37 °C. The changes of the storage modulus (G') and loss modulus (G'') were measured over an oscillation torque range of 0.1−100 rad/s. The morphology of the freeze-dried hydrogel was observed by scanning electron microscopy (SEM) (Micrion FEI PHILIPS). ImageJ was used to analyze SEM images. For UV irradiation, a xenon lamp source (CEL-S500, AuLight) equipped with filters was used to generate parallel monochromatic 365 nm light. A microplate reader (ELx 680, BioTek Instrument Inc.) was used to quantitatively determine cell viabilities, ALP activities, and ARS staining results. All digital photos were recorded with a camera (Canon EOS 550D). A laser scanning confocal microscope (Zeiss LSM 780) was used to observe cell microcosmic character. Activion 16 CT (Toshiba) was used to observe bone regeneration of the skull defect model.

2.3. Synthesis of nHAp-OA (oleic acid-modified nHAp) and nHAp-PEA (*O*-phosphorylethanolamine-modified nHAp). nHAp-OA and nHAp-PEA were synthesized using a hydrothermal route.[46,47] Typically, octadecylamine (0.5 g), oleic acid (4 mL), and ethanol (16 mL) were mixed together under agitation, followed by addition of a Ca(NO$_3$)$_2$ solution (0.067 g/mL). Then, a Na$_3$PO$_4$ solution (0.067 g/mL) was dropwise added and stirred for 5 min. Afterward, the mixture was transferred to a 50 mL Teflon hydrothermal reaction vessel sealed with thick steel items and autoclaved at 120 °C (hydrothermal method) for 8 h to obtain nHAp-OA.[46] Next, nHAp-OA (50 mg) was dispersed in ethanol (10 mL), and PEA (250 mg in 10 mL of distilled water) was added under vigorous stirring at 0 °C for 24 h to obtain the crude product. After being washed several times with deionized water, nHAp-PEA nanoparticles were finally obtained after lyophilization.

2.4. BMP-2 Peptide Immobilization and *in Vitro* Release. nHAp-PEA (200 mg) and BMP-2 peptide (340 μg) or FITC-BMP-2 peptide (400 μg) were dispersed in a PBS solution (10 mL, pH 7.4). Then, EDC (76.68 mg) and NHS (115.09 mg) were added at 0 °C, and the mixture was stirred at room temperature for 24 h. After centrifugation, the obtained nHAp-BMP-2 and nHAp-BMP-2-FITC were washed three times with both PBS and sterile water (10 mL for each time) to remove the excess BMP-2 peptides. The entire scrubbing solution was collected to determine the amount of peptide being grafted onto the surface of nHAp-PEA by the UV−vis absorption at 495 nm according to the standard curve of FITC-BMP-2. The collected products (nHAp-BMP-2 and nHAp-BMP-2-FITC) were freeze-dried and stored at −80 °C for further use. Besides, the mixture of BMP-2/BMP-2-FITC (0.185 wt %) and nHAp (named nHAp+BMP-2/nHAp+BMP-2-FITC) was prepared and stored at −80 °C for further use.

nHAp-BMP-2-FITC or nHAp+BMP-2-FITC (50 mg) was suspended in a plastic centrifuge tube with a PBS solution (5 mL, pH 7.4), and the tubes were shaken (100 rpm) at 37 °C to investigate BMP-2 peptide release *in vitro*. At predetermined time points, the mixture was centrifuged at 12000 rpm, 2 mL of the supernatant was removed, and the same volume of fresh PBS was added. The released amount of BMP-2 peptide was measured at 495 nm by a UV−vis spectrometer.

2.5. Synthesis of Gelatin Methacrylamide (GelMA). GelMA was prepared as previously described.[21,22] In short, gelatin (type A, 20 g) was dissolved in Dulbecco's phosphate-buffered saline (DPBS, pH 7.4) [10% (w/v)] at 50 °C under agitation, and then the temperature was increased to 60 °C with the addition of methacrylic anhydride (10 mL). Excess DPBS (40 °C) was used to stop the reaction after 3 h. The mixture was stirred for an additional 15 min before dialysis against distilled water using a dialysis bag with a molecular cutoff of 14 kDa for 7 days at 40 °C to remove the byproducts. Subsequently, the solution was freeze-dried, and the final product was kept at −80 °C. The yield of the purified product was 78.25%, and the detailed characterization is provided in Figure S1.

2.6. Synthesis of Four-Armed PEG$_{10K}$ Methacrylamide (four-armed PEGMA). First, four-armed PEG$_{10K}$-NH$_2$ (four-armed PEGNH$_2$) with four terminal amino groups was synthesized. Briefly, four-armed PEG (8 g) and anhydrous triethylamine (TEA, 1.784 mL) were dissolved in anhydrous methylene chloride (DCM, 40 mL) at 0 °C, followed by the addition of methanesulfonyl chloride (0.99 mL), and the reaction proceeded for 24 h. Then the terminal groups were turned into amino after reaction for 3 days in an ammonia solution (25%, 300 mL, containing 3.2 g of ammonium chloride). Second, four-armed PEG-NH$_2$ (5.2 g) was dissolved in preheated DPBS (pH 7.4, 50 °C) [10% (w/v)] followed by the addition of methacrylic anhydride (4 mL). After dialysis against distilled water using 3500 Da molecular cutoff dialysis tubing, four-armed PEGMA was obtained after freeze-drying. The yield of four-armed PEGMA was 80.32%, and the detailed characterization is provided in Figure S1.

2.7. Preparation and Swelling Ratio Test of the Gel/(nHAp-BMP-2) Composite. Photo initiator Irgacure 2959 [I2959, 0.5% (w/v)], GelMA [5.0% (w/v)], and four-armed PEGMA [2.5% (w/v)] were dissolved in a PBS solution (0.01 M, pH 7.4) followed by autoclaving at 120 °C for 20 min. Then nHAp-BMP-2/nHAp-BMP-2-FITC [0.4% (w/v)] was added after the precursor solution had cooled to room temperature. After being exposed to UV light (7.4 mW/cm^2, 365 nm) for 5 min, the bioactive nanoparticle/composite hydrogel [Gel/(nHAp-BMP-2)] was prepared. The hydrogel without nHAp (Gel), the hydrogel mixed with nHAp-PEA [Gel/(nHAp-PEA)], or the hydrogel mixed with nHAp and BMP-2 [Gel/(nHAp+BMP-2)] was also prepared and used as a control.

To test the swelling ratio, the freeze-dried composite hydrogels were immersed in ultrapure water at 37 °C in a constant-temperature incubator shaker (80 rpm).

2.8. Isolation and Culture of Rabbit BMSCs. New Zealand white rabbits (male, 2−3 weeks of age) were purchased from Jilin University. Rabbit bone marrow was extracted from tibial and femoral bone as described previously.[48−50] The monomer cells from the bone

marrow were separated using a Ficoll density cushion and centrifugation. The culture medium is low-glucose Dulbecco's modified Eagle's medium (DMEM, Gibco), supplemented with 15% fetal bovine serum (FBS, Gibco), 50 IU/mL streptomycin, and 50 IU/mL penicillin. Then, the BMSCs were cultured in medium at 37 °C under a 5% CO_2 atmosphere. Upon reaching 80% confluence, the cells were trypsinized and subcultured. The fourth to sixth passages were used for the following experiments.

2.9. Cell Viability, Proliferation, ALP Activity, and Mineralization of BMSCs Cultured with nHAp-BMP-2. The cell viability of BMSCs was assessed using the CCK-8 assay. Rabbit BMSCs were seeded in 96-well plates (100 μL, 5×10^3 cells/well) and incubated in 5% CO_2 at 37 °C overnight. nHAp-BMP-2, nHAp-PEA or nHAp and BMP-2 suspensions (100 μL) at different concentrations were then added and co-cultured. Then, CCK-8 (10 μL/well) was added, and the mixture incubated for an additional 4 h. Finally, the culture medium was measured by UV−vis absorption at 450 nm. BMSCs cultured without nanoparticles were used as a control, and the measurements were performed in triplicate.

The cell proliferation ability was studied by seeding BMSCs in 24-well plates (1 mL, 5×10^4 cells/well) and then incubated with nHAp-BMP-2 (100 μg/mL, 1 mL of DMEM) over time. CCK-8 (100 μL/well) was added, and after 4 h, the supernatant (150 μL/well) was transferred into a 96-well plate and measured by UV−vis absorption at 450 nm. The influence of nHAp-PEA or nHAp and BMP-2 on BMSCs was also tested. BMSCs cultured without nanoparticles were used as a control.

The ALP activity of BMSCs was evaluated by an ALP assay and a BCA protein assay. BMSCs (2 mL, 7.5×10^4 cells) were seeded in Petri dishes (60 mm diameter) and cultured with nHAp-BMP-2, nHAp-PEA, or nHAp and BMP-2 (100 μg/mL) in DMEM (low-glucose) for 4 days. Next, the medium was changed into osteoblast differentiation (OD) medium composed of DMEM (high-glucose), dexamethasone (7.84×10^{-2} μg/mL), sodium β-glycerophosphate (3.06 mg/mL), and ascorbic acid (0.05 mg/mL). After being induced for 7 and 14 days, the cells were lysed following the standard procedure. The lysate (100 μL/well) was added to a 96-well plate containing the substrate solution of the ALP assay kit, and 25 μL (per well) of the lysate was added to another 96-well plate containing the substrate solution of the BCA protein assay kit. After incubation at 37 °C for 30 min, the absorbance of each well was recorded to determine the ALP concentration, and the obtained value was normalized by the total protein concentration of the corresponding sample determined by the BCA protein assay. BMSCs cultured without OD medium were used as a control.

Mineralization of the induced BMSCs was evaluated both qualitatively and quantitatively by the Alizarin Red S staining method. BMSCs (2 mL, 7.5×10^4 cells) were seeded in Petri dishes (60 mm diameter) and cultured with nanoparticles (100 μg/mL) in DMEM (low-glucose) for 4 days. Next, the medium was changed to OD medium. After being induced for 14 days, BMSCs were fixed with 4% formalin for 10 min, and the fixed cells were incubated with a 2% (w/v) ARS solution at room temperature for 20 min. After the excess ARS solution had been removed, the samples were imaged by camera and magnified by an inversion fluorescence microscope. To quantify the amount of ARS, 10% acetic acid was added for overnight incubation and then centrifuged at 13000 rpm for 15 min. The supernatant was removed and neutralized with 10% ammonia. The optical density of the supernatant was measured by UV−vis absorption at 405 nm. BMSCs cultured without OD medium were used as a control.

2.10. Analysis of Intracellular Uptake. Rabbit BMSCs (2.5×10^4 cells/well) were seeded in a 24-well plate and incubated for 24 h. Next, BMSCs were exposed to nHAp-BMP-2-FITC in DMEM (100 μg/mL) for specific time points before being fixed with 4% formalin. Afterward, cells were permeated with 0.1% Triton X-100 for 10 min and incubated with 1% BSA for 30 min. The actin filaments of BMSCs were stained with phalloidin for 40 min, and nuclei were stained with Hoechst (10 μg/mL) for 6 min. Then, the samples were observed by confocal laser scanning microscopy (CLSM).

2.11. Spreading and Morphology of BMSCs in a Two-Dimensional (2D)/Three-Dimensional (3D) Culture. The cell viability of BMSCs cultured with different concentrations of I2959 was conducted with the CCK-8 assay. Briefly, BMSCs (3.5×10^3 cells, 100 μL/well) were seeded in a 96-well plate. After 24 h, different concentrations of I2929 (100 μL) were added, and the cells were further cultured for 24, 48, and 72 h. The cell viability of BMSCs was tested with the CCK-8 kit (10 μL/well).

For the 2D culture, the hydrogel precursor solution composed of GelMA, four-armed PEGMA, nHAp-BMP-2, and the photoinitiator (I2959) was added to a six-well plate (2 mL/well) to form the hydrogel disk after UV irradiation. Then, BMSCs [2.5×10^4 cells/mL in DMEM (low-glucose), 2 mL/well] were added on the surface of a fully cross-linked hydrogel.

For the 3D culture, BMSCs were first mixed with a hydrogel precursor solution (2.5×10^4 cells/mL, 2 mL/well) and then transferred to a six-well plate. The BMSC-laden hydrogels were quickly formed under UV irradiation. Then, DMEM (low-glucose, 2 mL/well) was added, and cells were incubated for 6 or 24 h. The actin filaments of BMSCs were stained red by phalloidin, and cell nuclei were stained blue by Hoechst. PBS washing was conducted after each step. Then, the samples were observed by CLSM.

2.12. 2D Proliferation of BMSCs Cultured on the Surface of the Hydrogel. The hydrogel precursor solution (1 mL/well) was added to a 12-well plate, and the hydrogel was formed *in situ*. Afterward, BMSCs (4.0×10^4 cells/well) were added on the hydrogel surface. Cell proliferation was assessed after 1, 3, and 5 days using the CCK-8 kit (150 μL/well).

For SEM observation, the cell-laden hydrogels were washed with PBS and fixed with 4% paraformaldehyde for 20 min before being freeze-dried. Then, the cell morphology on the hydrogel surface was checked. The medium was changed every 2 days, and three controls were set for each sample.

2.13. ARS Staining of BMSCs Cultured on the Hydrogel after Osteogenic Differentiation. The hydrogel was formed in a six-well plate by the method described above. Afterward, BMSCs (5×10^3 cells/mL in DMEM, 2 mL/well) were added and proliferated for 4 days. Then, the medium was changed to OD medium. After induction for 14 days, the hydrogels were washed three times with PBS and further immersed in 4% formalin for 20 min to fix the cells. Next, 1 mL of the ARS solution per well was added and kept at room temperature for 10 min. After the excess ARS had been removed, samples were imaged and magnified with a microscope. To quantify the amount of absorbed ARS, the cell-laden hydrogels were immersed in 10% acetic acid for 48 h and then centrifuged at 13000 rpm for 15 min. The supernatant was removed and neutralized with 10% ammonia. The optical density was measured. The non-induced BMSC-laden hydrogel without nanoparticles was used as a control.

2.14. Animals. Sprague-Dawley (SD) rats (male, 6 weeks of age, 180−200 g) were purchased from Jilin University. All rats were maintained under required conditions and had free access to food and water throughout the experiments. Their use for this study was approved by the Animal Ethics Committee of Changchun Institute of Applied Chemistry, Chinese Academy of Sciences.

2.15. *In Vivo* Degradation and Foreign Body Response Test of the Hydrogel. To assess the degradability and biocompatibility of the hydrogels *in vivo*, all the samples were implanted subcutaneously in the back of SD rats. At different time intervals, the rats were euthanized and the implantation materials were removed, observed, washed, and finally freeze-dried before being weighed. The subcutaneous fat and muscle tissues around the implantation were surgically removed and stored in 4% formalin. The inflammatory responses were evaluated by hematoxylin and eosin (H&E) staining, and each sample was tested in triplicate.

2.16. Implantation of the Hydrogel in a Skull Bone Defect. SD rats were randomized into four groups: Sham (control), Gel, Gel/(nHAp-PEA), and Gel/(nHAp-BMP-2). Before surgery, the rats were anesthetized with a 10% chloral hydrate solution, and then their heads were drilled to create a 5.0 mm diameter defect. After the calvarial disk had been removed, the hydrogels were formed *in situ* by UV
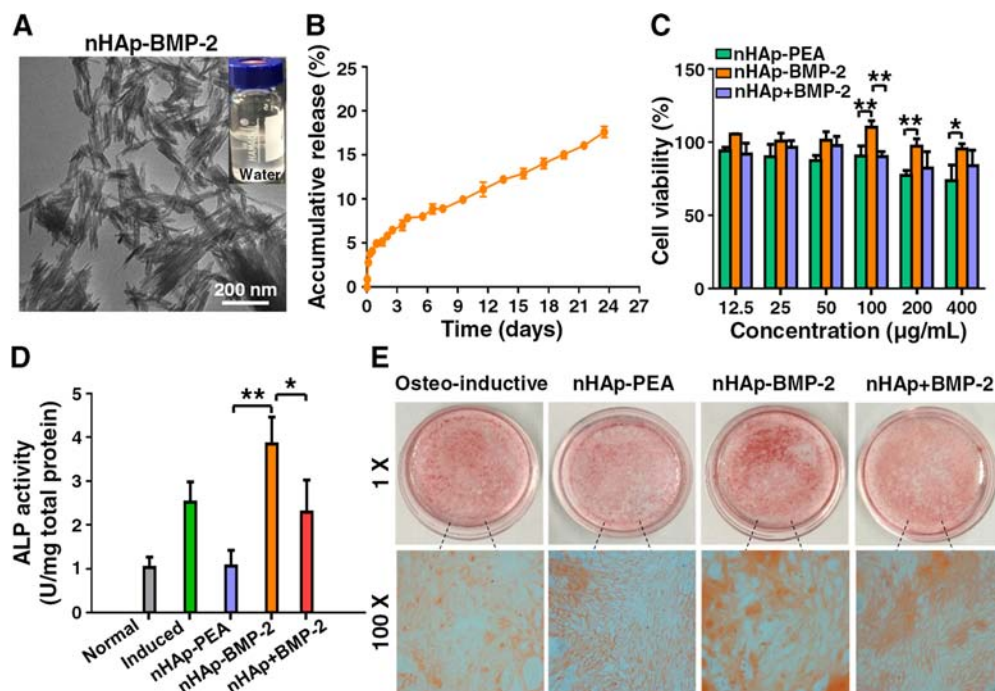
Figure 1. Characterization and bioactivity of nHAp-BMP-2. (A) TEM image of nHAp-BMP-2 and its dispersion in water. (B) BMP-2 peptide release profile of nHAp-BMP-2 at 37 °C. (C) Cell viability of BMSCs cultivated with nHAp-PEA, nHAp-BMP-2, or nHAp and BMP-2 for 68 h. (D) *In vitro* ALP activity of BMSCs cultured with various samples after induction for 14 days. (E) Mineralized matrix of BMSCs stained by ARS after induction for 14 days ($n = 3$; *$p < 0.05$, and **$p < 0.005$).

irradiation at 7.4 mW/cm^2 for 5 min. Next, the periosteum and rat skin were sutured. Four and 12 weeks after operation, the animals were euthanized and their head sections were scanned by Activion 16 CT to analyze bone volume and density. After 12 weeks, hydrogels along with the surrounding bone were harvested and fixed in 4% formalin and embedded in paraffin after decalcification. All the samples were stained with H&E and Trichrome Goldner to observe the new bone formation.

2.17. Statistical Analysis. The statistical difference between the control and experimental groups was analyzed by a paired Student's *t* test. Differences were considered statistically significant at the following levels: *$p < 0.05$; +$p < 0.05$; &$p < 0.05$; **$p < 0.005$. All experiments were performed at least three times, and the data are presented as means ± the standard deviation.

2.18. Data Avaliability. All relevant data included in this study are available from the corresponding author upon reasonable request.

3. RESULTS AND DISCUSSION

3.1. Characterization of nHAp-BMP-2 Nanoparticles. Oleic acid-modified nHAp (nHAp-OA) was prepared through the one-step hydrothermal reaction. The oleic acid was easily substituted with *O*-phosphorylethanolamine (PEA), and the aminated nHAp (nHAp-PEA) could be obtained via ligand exchange.[51] BMP-2 peptides were then covalently immobilized on nHAp-PEA through reaction with the help of 1-ethyl-3-[3-(dimethylamino)propyl]carbodiimide (EDC) and *N*-hydroxysuccinimide (NHS) (Scheme 1A and Figure S2). Fluorescent microscopy images of nHAp-BMP-2-FITC proved the successful covalent immobilization of BMP-2 (Figure S3). The amount of immobilized BMP-2 was determined to be 1.85 μg/mg based on the standard curve (Figure S4A), and approximately 92.35 wt % BMP-2 was successfully immobilized. Compared to nHAp-OA, nHAp-BMP-2 had a similar acicular morphology (Figure 1A and Figure S5). After peptide immobilization, nHAp-BMP-2 (1 mg/mL) exhibited good dispersibility in an aqueous solution (Figure 1A, inset).

Because of the strong coordination interaction between PEA and nHAp, the aminated nHAp was very stable, guaranteeing the slow release of BMP-2. To confirm the slow release of conjugated BMP-2 peptide from nHAp-BMP-2, the release time was prolonged to 4 weeks, and ~17.64% BMP-2 peptide was released on the 24th day (Figure 1B). In comparison, almost all the peptide was released in 24 h for the nHAp-PEA/BMP-2 mixed group (Figure S4B). This result illustrates that covalent bonding could slow the release of peptide.

The biocompatibility of nHAp-BMP-2 was assessed against BMSCs. As shown in Figure 1C, nHAp-BMP-2 exhibited cytocompatibility that was better than those of nHAp-PEA and nHAp with BMP-2, and no obvious cytotoxicity of nHAp-BMP-2 against BMSCs was observed even at 400 μg/mL. CLSM results further showed that nHAp-BMP-2-FITC was mainly distributed in the cytoplasm after being taken up, and no nucleus or cell morphology change was observed (Figure S6). In addition, the amount of BMSCs treated with nHAp-BMP-2 was 1.68 times that treated with nHAp and 1.23 times that treated with nHAp and BMP-2 after incubation for 3 days at 100 μg/mL (Figure S7). The alkaline phosphatase (ALP) is an important marker, which will be upregulated during the early stage of osteogenic differentiation of BMSCs.[52−54] As expected, nHAp-BMP-2 markedly enhanced the ALP activity on day 14 (Figure 1D). The ALP activity of nHAp-BMP-2-treated BMSCs was 3.63 times that of nHAp-PEA and 1.68 times that of nHAp+BMP-2, indicating that the endocytosis of nHAp-BMP-2 and free released BMP-2 can upregulate ALP expression in BMSCs. The calcium deposits secereted by osteogenic differentiated BMSCs were further studied by Alizarin Red S staining (ARS) (Figure 1E). Upon observation under a microscope, a larger area of calcium deposits (stained red) was observed in the whole cell matrix of the nHAp-BMP-2 group while only cellular outlines of other groups were
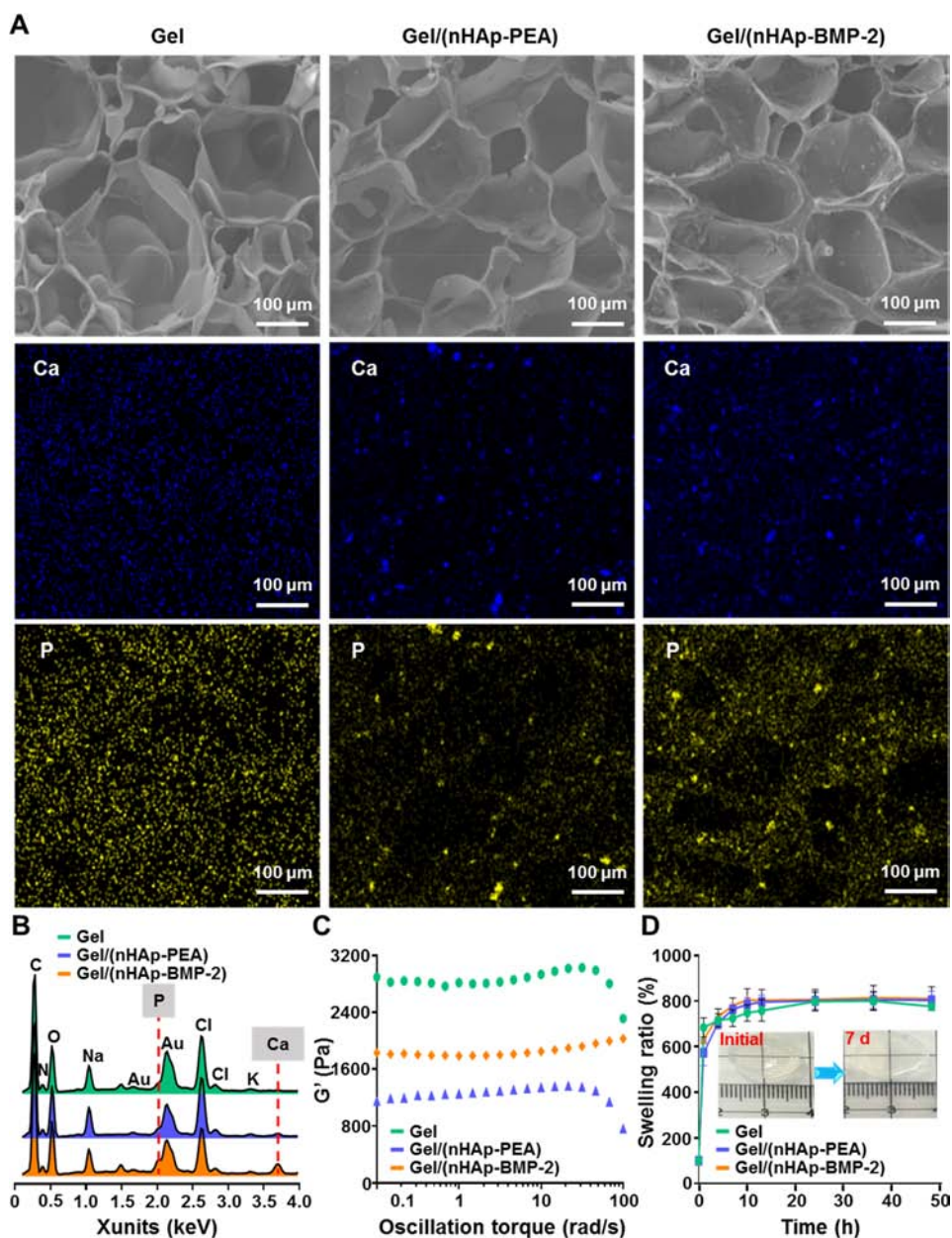
Figure 2. Physicochemical properties of the Gel/(nHAp-BMP-2) composite hydrogel. (A) Cross-sectional images of Gel, Gel/(nHAp-PEA), and Gel/(nHAp-BMP-2) after lyophilization and the corresponding element mappings of Ca and P. (B) EDX analysis of Gel, Gel/(nHAp-PEA), and Gel/(nHAp-BMP-2). (C) Storage modulus (G') of Gel, Gel/(nHAp-PEA), and Gel/(nHAp-BMP-2) measured in an oscillation torque (rad/s)-dependent model. (D) Equilibrium swelling property of freeze-dried Gel, Gel/(nHAp-PEA), and Gel/(nHAp-BMP-2) ($n = 3$).

stained red. In addition, the shape of nHAp-BMP-2-treated cells changed from a spindle to an irregular form accompanied by newly generated protrusions, and the size of BMSCs increased. The growth medium group ("Normal" in Figure S8A) showed no obvious calcium deposit even after 14 days, proving the effectiveness of the induction process. From the quantitative results, the nHAp-BMP-2 group showed 2.09-fold calcium deposits in BMSCs treated with nHAp-PEA and 1.81-fold in BMSCs treated with nHAp and BMP-2 (Figure S8B). Given the above, with the slowly released BMP-2 and improved biocompatibility, nHAp-BMP-2 greatly promoted the proliferation and differentiation of BMSCs, which established the biological foundation for further incorporating nHAp-BMP-2 into a gelatin hydrogel for bone regeneration.

3.2. Physicochemical Properties of the Gel/(nHAp-BMP-2) Composite Hydrogel. The Gel/(nHAp-BMP-2) composite hydrogel was developed by a facile UV cross-linking procedure (Figure S9). There were two main organic components of this hydrogel, in which GelMA was used to mimic the collagen matrix for cell growth and four-armed PEGMA [raw material: M_w = 9188, and PDI = 1.17 (Figure S10)] was used to adjust the hydrogel strength and degradation profile.

The element mapping on the fractured cross section of the Gel/(nHAp-BMP-2) composite showed a larger amount and a more homogeneous distribution of Ca and P elements, indicating better dispersibility of nHAp-BMP-2 than nHAp-PEA in the hydrogel and better organic/inorganic compatibility of the Gel/(nHAp-BMP-2) composite than of the Gel/
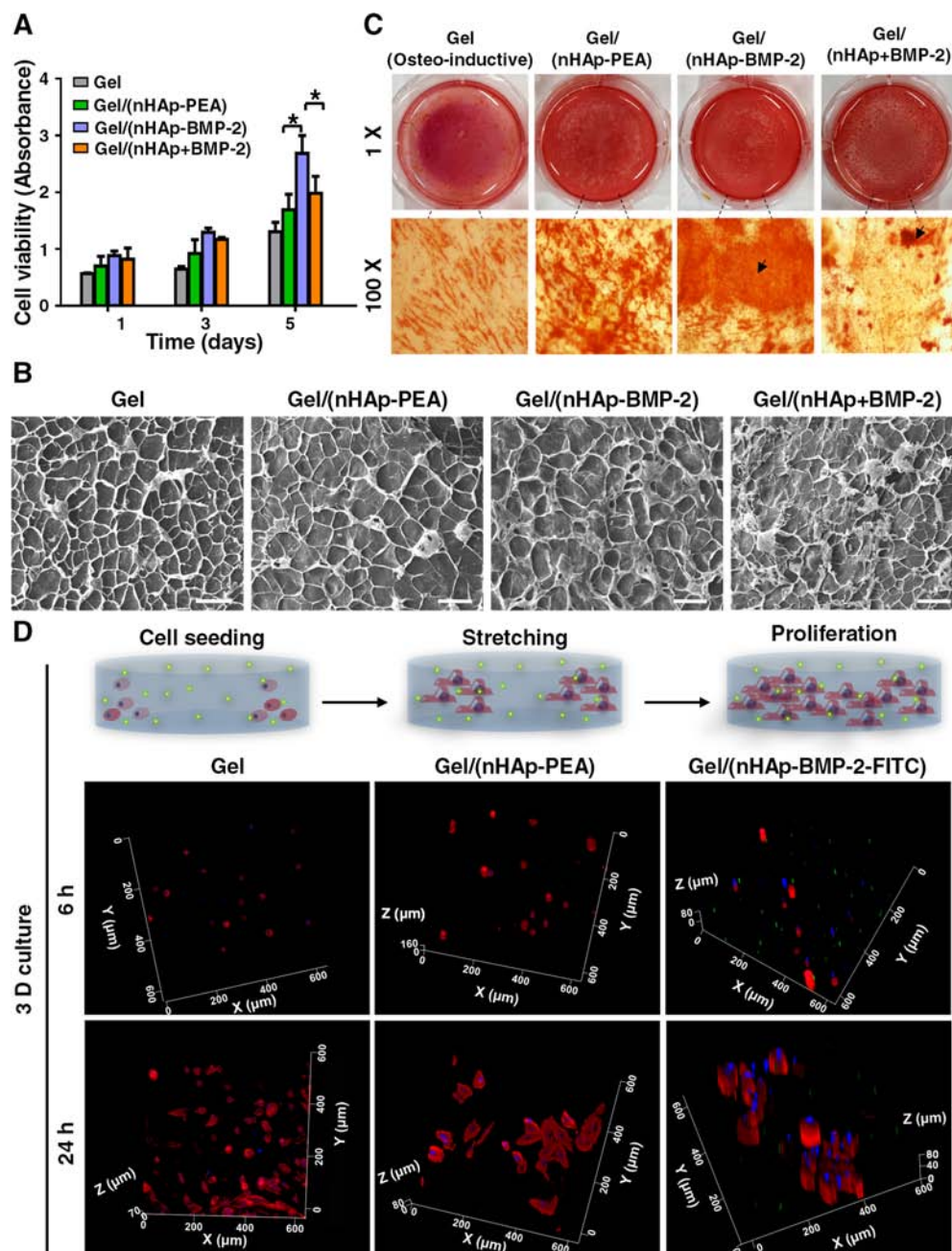
Figure 3. Evaluation of Gel/(nHAp-BMP-2) composite bioactivity *in vitro*. (A) Proliferation of BMSCs after a 2D culture on the surface of hydrogels [$n = 3$; *$p < 0.05$ vs Gel and Gel/(nHAp+BMP-2) group on the 5th day]. (B) SEM images of the BMSC-laden hydrogels after cell proliferation for 5 days (scale bar, 200 μm). (C) ARS staining of the mineralized matrix formed in BMSCs on a hydrogel surface after induction for 14 days. (D) Z-Stack CLSM images of BMSCs after a 3D culture within Gel, Gel/(nHAp-PEA), and Gel/(nHAp-BMP-2) for 6 and 24 h. F-Actin filaments were stained with 568 phalloidin (red); nuclei were stained with Hoechst (blue), and nHAp-BMP-2 was labeled with FITC (green).

(nHAp-PEA) composite (Figure 2A). From the corresponding energy dispersive X-ray (EDX) spectra shown in Figure 2B, it can be seen that mineral elements such as Ca and P were detected in both Gel/(nHAp-BMP-2) and Gel/(nHAp-PEA) composites, but not in Gel, and the mineral element content on the surface of the Gel/(nHAp-BMP-2) composite is higher than that of the Gel/(nHAp-PEA) composite.

The pore wall of the Gel/(nHAp-BMP-2) composite is thicker and rougher than that of the Gel/(nHAp-PEA) composite and Gel (Figure S11A). The pore size of the Gel/(nHAp-BMP-2) composite (132.2 nm) is slightly smaller than that of the Gel/(nHAp-PEA) composite (135.3 nm) (Figure

S11B). Incorporated with inorganic nanoparticles, both Gel/(nHAp-BMP-2) and Gel/(nHAp-PEA) composite hydrogels exhibited mechanical performance different from those of Gel (Figure 2C). It is reasonable that the influence of reduced light transmittance after incorporation of inorganic nanoparticles reduces the degree of cross-linking, which is the important influence factor for pore size and mechanical strength of the composite hydrogels.[29] Via the adjustment of the irradiation time, hydrogels with different mechanical strengths could be obtained (Figure S12). It is worth mentioning that, for the same light irradiation time (5 min), the Gel/(nHAp-BMP-2) composite presented a storage modulus (~1.8 kPa) much
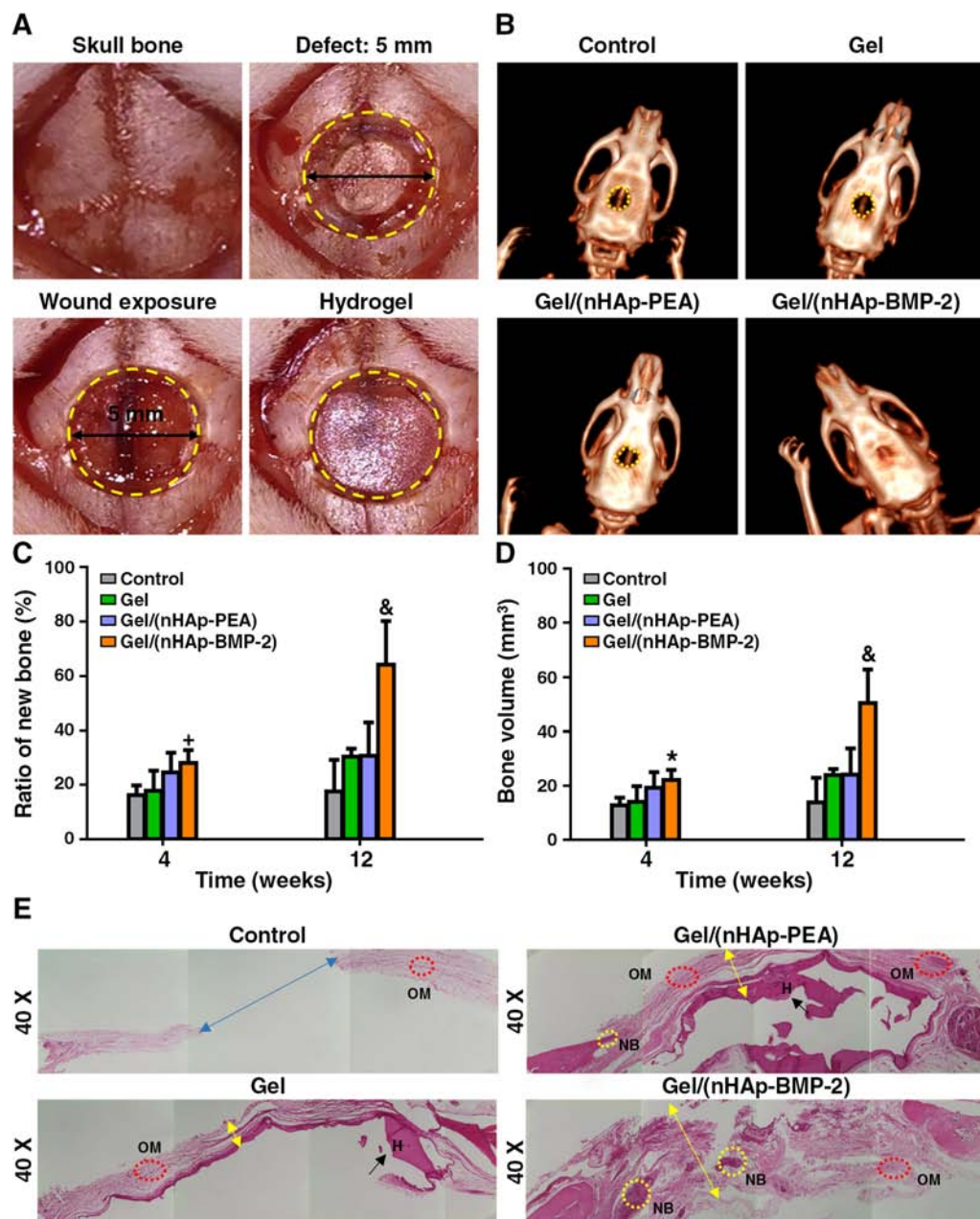
Figure 4. *In vivo* efficacy and mechanism of Gel/(nHAp-BMP-2) for bone regeneration on a rat's calvarial defect model. (A) Process of surgical operation to build the rat's calvarial defect model and hydrogel formed *in situ*. Briefly, the skin and periosteum were incised along with the skull bone exposure. Then a defect with a 5 mm diameter was introduced, and the calvarial disk was removed before the hydrogel forming within the defect. (B) CT images of the rat's calvarial defect model treated with Gel, Gel/(nHAp-PEA), and Gel/(nHAp-BMP-2) for 12 weeks. The untreated group was used as a control. (C) Ratio and (D) volume of new bone analyzed by CT signals ($n = 3$; *$p < 0.05$ vs control and Gel groups in weeks 4 and 12; +$p < 0.05$ vs the control group in week 4; &$p < 0.05$ vs all of the other groups in week 12). (E) H&E staining of the calvarial defect region after treatment with Gel, Gel/(nHAp-PEA), and Gel/(nHAp-BMP-2) for 12 weeks. The yellow arrows show the thickness of the osteoid matrix, and the blue arrow indicates the blank area in the defect of the control group [H, hydrogel remnant (black arrows); NB, new bone; OM, osteoid matrix].

higher than that of the Gel/(nHAp-PEA) composite (~1.2 kPa) at 10.0 rad/s. It is deemed that the chemical immobilization of BMP-2 on nHAp enhanced the compatibility between nanoparticles and polymers due to the exsistense of hydrogen bonding between BMP-2 and gelatin. Interestingly, it is observed that the addition of nHAp-BMP-2 had no influence on the swelling ratio (Figure 2D). The water absorptions of all hydrogel samples were nearly the same, more than 800 wt % after 40 h. Despite the fact that the weight

swelling ratio was so high, there was no significant change in the volume of the Gel/(nHAp-BMP-2) composite after its immersion in PBS (pH 7.4) for 1 week (Figure 2D, inset). The results demonstrated that the Gel/(nHAp-BMP-2) composite had an appropriate pore size and enhanced mechanical stability, guaranteeing the balance of a cell living microenvironment and a high degree of moisture retention for cell growth.

3.3. Cell Cytotoxicity, *in Vitro* Cell Proliferation, Differentiation, and Biomineralization of BMSCs on the Hydrogel Surface and a 3D Culture of BMSCs within the Hydrogel. The cell cytotoxicity of Gel/(nHAp-BMP-2) hydrogels was determined by the viability of BMSCs in a hydrogel leaching solution. As shown in Figure S13, initiator I2959 and a hydrogel leaching solution showed no cytotoxicity against BMSCs, indicating the superior biocompatibility and suitability of hydrogels for cell culture.

To determine the influence of the hydrogel microenvironment and bioactive BMP-2 peptide on cell adhesion, spread, proliferation, differentiation, and cell mineralization, BMSCs were cultured on the hydrogel surface (2D culture mode). After 2D mode culture for 6 h, BMSCs fully spread into a spindle shape and exhibited a healthy growth tendency on the Gel/(nHAp-BMP-2) composite, while most cells kept a spherical shape on the surface of Gel (Figure S14). BMSCs treated on the Gel/(nHAp-BMP-2) surface showed rates of proliferation 1.80- and 1.56-fold higher than those of Gel/(nHAp-PEA) and Gel/(nHAp+BMP-2) composites, respectively, during a 5 day cultivation (Figure 3A). SEM images of BMSCs on a hydrogel further confirmed these results (Figure 3B). A much larger mumber of cells and a higher level of cellular aggregation were obeserved on the Gel/(nHAp-BMP-2) composite. All the results demonstrated that, except for the positive effect from BMP-2 peptide, the rough surface structure and suitable mechanical property of the Gel/(nHAp-BMP-2) composite were also benefitcal to cell adhesion and living.

The biomineralization of differentiated BMSCs in osteo-genic inductive media was characterized by Alizarin Red S staining, and these results demonstrated that the inclusion of nHAp-BMP-2 in a hydrogel could accelerate cell mineraliza-tion. Under a microscope, the calcium deposition amount of BMSCs on the surface of the Gel/(nHAp-BMP-2) composite was much larger than that on the Gel/(nHAp+BMP-2) and Gel/(nHAp-PEA) composites (Figure S15). Noticeably, obvious flocking red areas (black arrows) were found only in the Gel/(nHAp-BMP-2) group (Figure 3C), which indicated that the Gel/(nHAp-BMP-2) composite stimulated the calcium node forming of osteoblasts *in vitro*.

BMSCs were further cultured within the hydrogels (3D culture mode) to simulate the living environment of BMSCs in tissues,[55,56] and the BMSCs in the hydrogels were visualized by a Z-stack CLSM method. As shown in Figure 3D, although the cells did not spread out after cell seeding for 6 h, the cell morphologies of different samples were significantly different from each other after 24 h. BMSCs were completely outstretched within Gel/(nHAp-BMP-2) and Gel/(nHAp-PEA) composites, while most cells were still in an oblate shape within Gel (Figure 3D). More interestingly, the cells showed quite different growth patterns in 2D and 3D culture modes. In a 2D culture, BMSCs spread out first and then migrated together to form cell clusters. In contrast, the cells tended to scatter apart from each other and become larger in 3D cell culture mode. Even though the growth of 3D-cultured cells may be hindered by the surrounding microenvironment, BMSCs exhibited a well-spread morphology within the Gel/(nHAp-BMP-2) and Gel/(nHAp-PEA) composites. All results indicated that, after incorporating nHAp-BMP-2, the Gel/(nHAp-BMP-2) composite exhibited excellent biological abilities, such as promoting cell spreading, proliferation, differentiation, and enhancing calcium deposition.

3.4. *In Vivo* Degradation and Biocompatibility of the Hydrogel. To investigate the *in vivo* performance of the Gel/(nHAp-BMP-2) composite, we evaluated its degradation profile and foreign body response by implanting the hydrogel in the subcutaneous tissue of SD rats. After making incisions in the skin of rats, we observed the status and size of the hydrogels every 2 weeks until they disappeared (Figure S16A). After 35 days, the implants were taken out and freeze-dried to test the accurate remaining mass of the materials. The Gel/(nHAp-BMP-2) and Gel/(nHAp-PEA) composites (∼17 wt % of its initial weight remained) degraded slightly faster than Gel, the level of which remained ∼20 wt % (Figure S17). The results suggest that along with the organic polymer degradation, the loaded nanoparticles could be released from the hydrogel. H&E staining of skin slices around the hydrogels was also performed to evaluate the foreign body response (Figure S16B). Initially, a considerable number of inflamma-tory cells existed on the edge of skin tissues (black arrows) because of the common inflammatory response, and no obvious tissue edema or necrosis was observed. Then the inflammation disappeared with the degradation of the hydrogel, and the histology of skin tissues was restored to normal in the fifth week, indicating the good biocompatibility of the Gel/(nHAp-BMP-2) composite *in vivo*.

3.5. Skull Bone Regeneration after Treatment with Hydrogels. The bone regeneration efficacy of Gel/(nHAp-BMP-2) hydrogels was evaluated on a rat calvarial defect model (Figure 4A). Hydrogels were formed *in situ* by UV irradiation at 7.4 mW/cm^2 for 5 min after injection of the composite solution into the defect (Figure S18). The bone regeneration efficacy was observed *in situ* by CT scanning. After hydrogel treatment for only a month, the Gel/(nHAp-BMP-2) composite already exhibited a better bone regener-ation efficacy with a higher new bone density compared to those of the Gel and Gel/(nHAp-PEA) composites (Figure S19). Excitingly, after treatment for 12 weeks, the Gel/(nHAp-BMP-2) composite displayed the best bone healing effect (Figure 4B). The new bone volume and the ratio of new bone to total defect area after Gel/(nHAp-BMP-2) composite treatment (50.54 ± 13.51 mm^3 and 64.38 ± 17.22%, respectively) were much higher than those values after treatment with the Gel/(nHAp-PEA) composite (24.2 ± 10.62 mm^3 and 30.77 ± 13.53%, respectively) and Gel (23.9 ± 2.62 mm^3 and 30.48 ± 3.34%, respectively) (Figure 4C,D). In contrast, the untreated group exhibits only bony bridging at the defect border (new bone volume of 13.84 ± 9.50 mm^3 and ratio of new bone to total defect area of 17.63 ± 12.10%).

Twelve weeks after implantation, bone sections surrounding implants were isolated from rats, and Trichrome Goldner staining and H&E staining were performed. From the Trichrome Goldner staining results (Figure S20), a layer of active osteoblasts embedded within the osteoid matrix (red circle) appeared on the top rim of the defect in treatment groups, and the Gel/(nHAp-BMP-2) group showed extensive and many more regions of new mature bone formation (yellow circle) than the others. In H&E staining images, the area of the osteoid matrix in the Gel/(nHAp-BMP-2) composite group was also larger than that of the other two groups (Figure 4E). Furthermore, new mature bone showed up along with the bottom edge of the defect in the Gel/(nHAp-BMP-2) composite group, which was not seen in the Gel or Gel/(nHAp-PEA) composite groups. These results further confirmed that the covalent immobilization of BMP-2 onto

nHAp provided the Gel/(nHAp-BMP-2) composite with a stem cell friendly microenvironment. To be specific, considerable mechanical stability due to the compatibility between organic and inorganic components and sustainable bioactivity due to bioactivity preservation and slow release of BMP-2 were favorable for stem cells to re-home, proliferate, and osteogenicly differentiate around the implanted hydrogel. In contrast, the defect area in the untreated group was primarily filled, with none marked bone formation, indicating the reliability of the animal model we used.

4. CONCLUSION

In summary, for the first time, a bone morphogenetic protein-2 (BMP-2) peptide covalently immobilized to nano-hydroxyapatite (nHAp-BMP-2) was synthesized. Then, a mechanically enhanced and biologically activated Gel/(nHAp-BMP-2) composite hydrogel was further developed by UV cross-linking of GelMA and four-armed PEGMA with the addition of bioactive nHAp-BMP-2. On one hand, the covalent bonding of the bioactive BMP-2 onto nHAp not only conferred upon the Gel/(nHAp-BMP-2) composite an enhanced storage modulus due to the improved compatibility between inorganic particles and organic molecules but also had a negligible impact on the swelling property, keeping the stable form during cell cultivation. On the other hand, covalent immobilization of BMP-2 onto nHAp preserved the bioactivity of BMP-2 by protecting the peptide being lysed by proteinases *in vivo* and reduced the bad side effects caused by burst release of large doses of BMP-2. The slow release of BMP-2 endowed the Gel/(nHAp-BMP-2) composite hydrogel with sustainable bioactivity that provides an outstanding bioactive microenvironment for attachment, proliferation, and osteogenic differentiation of stem cells. In addition, the Gel/(nHAp-BMP-2) composite could upregulate ALP expression, accelerate the formation of calcium deposits in BMSCs, and promote new bone formation on a rat skull bone defect model. Therefore, we believe that the Gel/(nHAp-BMP-2) composite may be used as a matrix for stem cell therapy and has great potential to be used for bone regeneration.

■ ASSOCIATED CONTENT

Ⓢ Supporting Information

The Supporting Information is available free of charge on the ACS Publications website at DOI: 10.1021/acs.biomac.8b00707.

Supplemental methods, Schemes S1, Figures S1−S20 (PDF)

■ AUTHOR INFORMATION

Corresponding Authors
*E-mail: east@ciac.ac.cn.
*E-mail: ybhuang@ciac.ac.cn.
ORCID Ⓞ
Xuesi Chen: 0000-0003-3542-9256
Dongfang Zhou: 0000-0002-8381-7440
Yubin Huang: 0000-0002-5212-318X

Author Contributions

N.S., D.Z., and Y.H. designed the study. N.S. performed and analyzed all experiments and wrote the manuscript. Y.G. operated the CT scanner and analyzed the data. H.Z. performed the mechanical strength test of the hydrogels and rheological data analysis. X.L. performed histology analysis. J.G. helped write the manuscript. D.Z. and X.C. calibrated the manuscript.

Notes

The authors declare no competing financial interest.

■ ABBREVIATIONS

nHAp-BMP-2, bone morphogenetic protein-2 covalently immobilized to nano-hydroxyapatite; GelMA, gelatin methacrylamide; four-armed PEGMA, four-armed PEG methacrylamide; BMSCs, bone marrow mesenchymal stem cells; BMPs, bone morphogenetic proteins; TGF-β, transforming growth factors β; PDGF, platelet-derived growth factor; IGF, insulin-like growth factor; BMP-2, bone morphogenetic protein 2; nHAp, nano-hydroxyapatite; PEA, O-phosphorylethanolamine; EDC, 1-ethyl-3-[3-(dimethylamino)propyl]carbodiimide; NHS, N-hydroxysuccinimide; ARS, Alizarin Red S; four-armed PEG, four-armed PEG$_{10K}$-OH; CCK-8, cell counting kit-8; FT-IR, Fourier transform infrared; XPS, X-ray photoelectron spectroscopy; TEM, transmission electron microscopy; SEM, scanning electron microscopy; ALP, alkaline phosphatase; nHAp-OA, sodium linoleate-modified nHAp; nHAp-PEA, O-phosphorylethanolamine-modified nHAp; SD, Sprague-Dawley; CLSM, confocal laser scanning microscopy.

■ REFERENCES

(1) Xu, B.; Zheng, P.; Gao, F.; Wang, W.; Zhang, H.; Zhang, X.; Feng, X.; Liu, W. A Mineralized High Strength and Tough Hydrogel for Skull Bone Regeneration. *Adv. Funct. Mater.* **2017**, *27* (4), 1604327.

(2) Swami, A.; Reagan, M. R.; Basto, P.; Mishima, Y.; Kamaly, N.; Glavey, S.; Zhang, S.; Moschetta, M.; Seevaratnam, D.; Zhang, Y.; Liu, J.; Memarzadeh, M.; Wu, J.; Manier, S.; Shi, J.; Bertrand, N.; Lu, Z. N.; Nagano, K.; Baron, R.; Sacco, A.; Roccaro, A. M.; Farokhzad, O. C.; Ghobrial, I. M. Engineered nanomedicine for myeloma and bone microenvironment targeting. *Proc. Natl. Acad. Sci. U. S. A.* **2014**, *111* (28), 10287−92.

(3) Ilyas, A.; Odatsu, T.; Shah, A.; Monte, F.; Kim, H. K.; Kramer, P.; Aswath, P. B.; Varanasi, V. G. Amorphous Silica: A New Antioxidant Role for Rapid Critical-Sized Bone Defect Healing. *Adv. Healthcare Mater.* **2016**, *5* (17), 2199−213.

(4) Liu, Y.; Liu, S.; Luo, D.; Xue, Z.; Yang, X.; Gu, L.; Zhou, Y.; Wang, T. Hierarchically Staggered Nanostructure of Mineralized Collagen as a Bone-Grafting Scaffold. *Adv. Mater.* **2016**, *28* (39), 8740−8748.

(5) Pina, S.; Oliveira, J. M.; Reis, R. L. Natural-based nanocomposites for bone tissue engineering and regenerative medicine: a review. *Adv. Mater.* **2015**, *27* (7), 1143−69.

(6) Baker, R. M.; Tseng, L. F.; Iannolo, M. T.; Oest, M. E.; Henderson, J. H. Self-deploying shape memory polymer scaffolds for grafting and stabilizing complex bone defects: A mouse femoral segmental defect study. *Biomaterials* **2016**, *76*, 388−98.

(7) Chen, G.; Dong, C.; Yang, L.; Lv, Y. 3D Scaffolds with Different Stiffness but the Same Microstructure for Bone Tissue Engineering. *ACS Appl. Mater. Interfaces* **2015**, *7* (29), 15790−802.

(8) Feinle, A.; Elsaesser, M. S.; Husing, N. Sol-gel synthesis of monolithic materials with hierarchical porosity. *Chem. Soc. Rev.* **2016**, *45*, 3377−3399.

(9) Shi, L.; Wang, F.; Zhu, W.; Xu, Z.; Fuchs, S.; Hilborn, J.; Zhu, L.; Ma, Q.; Wang, Y.; Weng, X.; Ossipov, D. A. Self-Healing Silk Fibroin-Based Hydrogel for Bone Regeneration: Dynamic Metal-Ligand Self-Assembly Approach. *Adv. Funct. Mater.* **2017**, *27* (37), 1700591.

(10) Arun Kumar, R.; Sivashanmugam, A.; Deepthi, S.; Iseki, S.; Chennazhi, K. P.; Nair, S. V.; Jayakumar, R. Injectable Chitin-Poly(epsilon-caprolactone)/Nanohydroxyapatite Composite Micro-gels Prepared by Simple Regeneration Technique for Bone Tissue Engineering. *ACS Appl. Mater. Interfaces* **2015**, *7* (18), 9399−9409.

(11) Yin, Y.; Wu, C.; Wang, J.; Song, F.; Yue, W.; Zhong, W. A simply triggered peptide-based hydrogel as an injectable nanocarrier of tanshinone IIA and tanshinones. *Chem. Commun.* **2017**, *53*, 529−532.

(12) Zhai, X.; Ma, Y.; Hou, C.; Gao, F.; Zhang, Y.; Ruan, C.; Pan, H.; Lu, W. W.; Liu, W. 3D-Printed High Strength Bioactive Supramolecular Polymer/Clay Nanocomposite Hydrogel Scaffold for Bone Regeneration. *ACS Biomater. Sci. Eng.* **2017**, *3* (6), 1109−1118.

(13) Huang, W.; Wang, Y.; Chen, Y.; Zhao, Y.; Zhang, Q.; Zheng, X.; Chen, L.; Zhang, L. Strong and Rapidly Self-Healing Hydrogels: Potential Hemostatic Materials. *Adv. Healthcare Mater.* **2016**, *5* (21), 2813−3822.

(14) Guo, J.; Xie, Z.; Tran, R. T.; Xie, D.; Jin, D.; Bai, X.; Yang, J. Click chemistry plays a dual role in biodegradable polymer design. *Adv. Mater.* **2014**, *26* (12), 1906−1911.

(15) Chen, R.; Wang, J.; Liu, C. Biomaterials Act as Enhancers of Growth Factors in Bone Regeneration. *Adv. Funct. Mater.* **2016**, *26* (48), 8810−8823.

(16) Ren, K.; Cui, H.; Xu, Q.; He, C.; Li, G.; Chen, X. Injectable Polypeptide Hydrogels with Tunable Microenvironment for 3D Spreading and Chondrogenic Differentiation of Bone-Marrow-Derived Mesenchymal Stem Cells. *Biomacromolecules* **2016**, *17* (12), 3862−3871.

(17) Tseng, T. C.; Tao, L.; Hsieh, F. Y.; Wei, Y.; Chiu, I. M.; Hsu, S. H. An Injectable, Self-Healing Hydrogel to Repair the Central Nervous System. *Adv. Mater.* **2015**, *27* (23), 3518−3524.

(18) Kim, J.; Staunton, J. R.; Tanner, K. Independent Control of Topography for 3D Patterning of the ECM Microenvironment. *Adv. Mater.* **2016**, *28* (1), 132−137.

(19) Dikina, A. D.; Almeida, H. V.; Cao, M.; Kelly, D. J.; Alsberg, E. Scaffolds Derived from ECM Produced by Chondrogenically Induced Human MSC Condensates Support Human MSC Chondrogenesis. *ACS Biomater. Sci. Eng.* **2017**, *3* (7), 1426−1436.

(20) Lata, J. P.; Guo, F.; Guo, J.; Huang, P. H.; Yang, J.; Huang, T. J. Surface Acoustic Waves Grant Superior Spatial Control of Cells Embedded in Hydrogel Fibers. *Adv. Mater.* **2016**, *28* (39), 8632−8638.

(21) Nichol, J. W.; Koshy, S. T.; Bae, H.; Hwang, C. M.; Yamanlar, S.; Khademhosseini, A. Cell-laden microengineered gelatin meth-acrylate hydrogels. *Biomaterials* **2010**, *31* (21), 5536−5544.

(22) Shin, S. R.; Zihlmann, C.; Akbari, M.; Assawes, P.; Cheung, L.; Zhang, K.; Manoharan, V.; Zhang, Y. S.; Yuksekkaya, M.; Wan, K. T.; Nikkhah, M.; Dokmeci, M. R.; Tang, X. S.; Khademhosseini, A. Reduced Graphene Oxide-GelMA Hybrid Hydrogels as Scaffolds for Cardiac Tissue Engineering. *Small* **2016**, *12* (27), 3677−3689.

(23) Ren, Z.; Wang, Y.; Ma, S.; Duan, S.; Yang, X.; Gao, P.; Zhang, X.; Cai, Q. Effective Bone Regeneration Using Thermosensitive Poly(N-Isopropylacrylamide) Grafted Gelatin as Injectable Carrier for Bone Mesenchymal Stem Cells. *ACS Appl. Mater. Interfaces* **2015**, *7* (34), 19006−19015.

(24) Hassanzadeh, P.; Kazemzadeh-Narbat, M.; Rosenzweig, R.; Zhang, X.; Khademhosseini, A.; Annabi, N.; Rolandi, M. Ultrastrong and Flexible Hybrid Hydrogels based on Solution Self-Assembly of Chitin Nanofibers in Gelatin Methacryloyl (GelMA). *J. Mater. Chem. B* **2016**, *4*, 2539−2543.

(25) Kerscher, P.; Kaczmarek, J. A.; Head, S. E.; Ellis, M. E.; Seeto, W. J.; Kim, J.; Bhattacharya, S.; Suppiramaniam, V.; Lipke, E. A. Direct Production of Human Cardiac Tissues by Pluripotent Stem Cell Encapsulation in Gelatin Methacryloyl. *ACS Biomater. Sci. Eng.* **2017**, *3* (8), 1499−1509.

(26) Zhang, J.; Jia, J.; Kim, J. P.; Shen, H.; Yang, F.; Zhang, Q.; Xu, M.; Bi, W.; Wang, X.; Yang, J.; Wu, D. Ionic Colloidal Molding as a Biomimetic Scaffolding Strategy for Uniform Bone Tissue Regeneration. *Adv. Mater.* **2017**, *29* (17), 1605546.

(27) Bhuiyan, D.; Jablonsky, M. J.; Kolesov, I.; Middleton, J.; Wick, T. M.; Tannenbaum, R. Novel synthesis and characterization of a collagen-based biopolymer initiated by hydroxyapatite nanoparticles. *Acta Biomater.* **2015**, *15* (15), 181−190.

(28) Wang, Z.; Xu, Y.; Wang, Y.; Ito, Y.; Zhang, P.; Chen, X. Enhanced in Vitro Mineralization and in Vivo Osteogenesis of Composite Scaffolds through Controlled Surface Grafting of L-Lactic Acid Oligomer on Nanohydroxyapatite. *Biomacromolecules* **2016**, *17* (3), 818−829.

(29) Xavier, J. R.; Thakur, T.; Desai, P.; Jaiswal, M. K.; Sears, N.; Cosgriff-Hernandez, E.; Kaunas, R.; Gaharwar, A. K. Bioactive Nanoengineered Hydrogels for Bone Tissue Engineering: A Growth-Factor-Free Approach. *ACS Nano* **2015**, *9* (3), 3109−3118.

(30) Singh, R. K.; Jin, G. Z.; Mahapatra, C.; Patel, K. D.; Chrzanowski, W.; Kim, H. W. Mesoporous Silica-Layered Biopolymer Hybrid Nanofibrous Scaffold: A Novel Nanobiomatrix Platform for Therapeutics Delivery and Bone Regeneration. *ACS Appl. Mater. Interfaces* **2015**, *7* (15), 8088−8098.

(31) Deng, C.; Yao, Q.; Feng, C.; Li, J.; Wang, L.; Cheng, G.; Shi, M.; Chen, L.; Chang, J.; Wu, C. 3D Printing of Bilineage Constructive Biomaterials for Bone and Cartilage Regeneration. *Adv. Funct. Mater.* **2017**, *27* (36), 1703117.

(32) Zhou, R.; Wei, D.; Cao, J.; Feng, W.; Cheng, S.; Du, Q.; Li, B.; Wang, Y.; Jia, D.; Zhou, Y. Synergistic effects of surface chemistry and topologic structure from modified microarc oxidation coatings on Ti implants for improving osseointegration. *ACS Appl. Mater. Interfaces* **2015**, *7* (16), 8932−8941.

(33) Takizawa, T.; Nakayama, N.; Haniu, H.; Aoki, K.; Okamoto, M.; Nomura, H.; Tanaka, M.; Sobajima, A.; Yoshida, K.; Kamanaka, T.; Ajima, K.; Oishi, A.; Kuroda, C.; Ishida, H.; Okano, S.; Kobayashi, S.; Kato, H.; Saito, N. Titanium Fiber Plates for Bone Tissue Repair. *Adv. Mater.* **2018**, *30* (4), 1703608.

(34) Jo, Y. K.; Choi, B. H.; Kim, C. S.; Cha, H. J. Diatom-Inspired Silica Nanostructure Coatings with Controllable Microroughness Using an Engineered Mussel Protein Glue to Accelerate Bone Growth on Titanium-Based Implants. *Adv. Mater.* **2017**, *29* (46), 1704906.

(35) Kawecki, F.; Clafshenkel, W. P.; Fortin, M.; Auger, F. A.; Fradette, J. Biomimetic Tissue-Engineered Bone Substitutes for Maxillofacial and Craniofacial Repair: The Potential of Cell Sheet Technologies. *Adv. Healthcare Mater.* **2018**, *7*, 1700919.

(36) Bilem, I.; Chevallier, P.; Plawinski, L.; Sone, E. D.; Durrieu, M.-C.; Laroche, G. Interplay of Geometric Cues and RGD/BMP-2 Crosstalk in Directing Stem Cell Fate. *ACS Biomater. Sci. Eng.* **2017**, *3* (10), 2514−2523.

(37) Kim, H. Y.; Lee, J. H.; Yun, J. W.; Park, J. H.; Park, B. W.; Rho, G. J.; Jang, S. J.; Park, J. S.; Lee, H. C.; Yoon, Y. M.; Hwang, T. S.; Lee, D. H.; Byun, J. H.; Oh, S. H. Development of Porous Beads to Provide Regulated BMP-2 Stimulation for Varying Durations: In Vitro and In Vivo Studies for Bone Regeneration. *Biomacromolecules* **2016**, *17* (5), 1633−1642.

(38) Dang, P. N.; Dwivedi, N.; Yu, X.; Phillips, L.; Bowerman, C.; Murphy, W. L.; Alsberg, E. Guiding Chondrogenesis and Osteo-genesis with Mineral-Coated Hydroxyapatite and BMP-2 Incorporated within High-Density hMSC Aggregates for Bone Regeneration. *ACS Biomater. Sci. Eng.* **2016**, *2* (1), 30−42.

(39) Paul, A.; Manoharan, V.; Krafft, D.; Assmann, A.; Uquillas, J. A.; Shin, S. R.; Hasan, A.; Hussain, M. A.; Memic, A.; Gaharwar, A. K.; Khademhosseini, A. Nanoengineered biomimetic hydrogels for guiding human stem cell osteogenesis in three dimensional micro-environments. *J. Mater. Chem. B* **2016**, *4*, 3544−3554.

(40) Li, L.; Zhou, G.; Wang, Y.; Yang, G.; Ding, S.; Zhou, S. Controlled dual delivery of BMP-2 and dexamethasone by nano-

particle-embedded electrospun nanofibers for the efficient repair of critical-sized rat calvarial defect. *Biomaterials* **2015**, *37*, 218−229.

(41) Zhou, X.; Feng, W.; Qiu, K.; Chen, L.; Wang, W.; Nie, W.; Mo, X.; He, C. BMP-2 Derived Peptide and Dexamethasone Incorporated Mesoporous Silica Nanoparticles for Enhanced Osteogenic Differentiation of Bone Mesenchymal Stem Cells. *ACS Appl. Mater. Interfaces* **2015**, *7* (29), 15777−15789.

(42) Cui, W.; Liu, Q.; Yang, L.; Wang, K.; Sun, T.; Ji, Y.; Liu, L.; Yu, W.; Qu, Y.; Wang, J.; Zhao, Z.; Zhu, J.; Guo, X. Sustained Delivery of BMP-2-Related Peptide from True Bone Ceramics/Hollow Mesoporous Silica Nanoparticles Scaffold for Bone Tissue Regeneration. *ACS Biomater. Sci. Eng.* **2018**, *4* (1), 211−221.

(43) Choi, W. I.; Kamaly, N.; Riol-Blanco, L.; Lee, I. H.; Wu, J.; Swami, A.; Vilos, C.; Yameen, B.; Yu, M.; Shi, J.; Tabas, I.; von Andrian, U. H.; Jon, S.; Farokhzad, O. C. A solvent-free thermosponge nanoparticle platform for efficient delivery of labile proteins. *Nano Lett.* **2014**, *14* (11), 6449−55.

(44) Kim, T. H.; Singh, R. K.; Kang, M. S.; Kim, J. H.; Kim, H. W. Gene delivery nanocarriers of bioactive glass with unique potential to load BMP2 plasmid DNA and to internalize into mesenchymal stem cells for osteogenesis and bone regeneration. *Nanoscale* **2016**, *8*, 8300−8311.

(45) Kim, M. J.; Lee, B.; Yang, K.; Park, J.; Jeon, S.; Um, S. H.; Kim, D. I.; Im, S. G.; Cho, S. W. BMP-2 peptide-functionalized nanopatterned substrates for enhanced osteogenic differentiation of human mesenchymal stem cells. *Biomaterials* **2013**, *34* (30), 7236−7246.

(46) Wang, X.; Zhuang, J.; Peng, Q.; Li, Y. D. Liquid−Solid−Solution Synthesis of Biomedical Hydroxyapatite Nanorods. *Adv. Mater.* **2006**, *18*, 2031−2034.

(47) Zhao, Y.; Shi, L.; Fang, J.; Feng, X. Bio-nanoplatforms based on carbon dots conjugating with F-substituted nano-hydroxyapatite for cellular imaging. *Nanoscale* **2015**, *7*, 20033−20041.

(48) Boo, L.; Selvaratnam, L.; Tai, C. C.; Ahmad, T. S.; Kamarul, T. Expansion and preservation of multipotentiality of rabbit bone-marrow derived mesenchymal stem cells in dextran-based microcarrier spin culture. *J. Mater. Sci.: Mater. Med.* **2011**, *22* (5), 1343−1356.

(49) Bakhtina, A.; Tohfafarosh, M.; Lichtler, A.; Arinzeh, T. L. Characterization and differentiation potential of rabbit mesenchymal stem cells for translational regenerative medicine. *In Vitro Cell. Dev. Biol.: Anim.* **2014**, *50* (3), 251−260.

(50) Tan, S. L.; Ahmad, T. S.; Selvaratnam, L.; Kamarul, T. Isolation, characterization and the multi-lineage differentiation potential of rabbit bone marrow-derived mesenchymal stem cells. *J. Anat.* **2013**, *222* (4), 437−450.

(51) Zhou, R.; Li, M.; Wang, S.; Wu, P.; Wu, L.; Hou, X. Low-toxic Mn-doped ZnSe@ZnS quantum dots conjugated with nano-hydroxyapatite for cell imaging. *Nanoscale* **2014**, *6*, 14319−14325.

(52) Cao, F.-Y.; Long, Y.; Wang, S.-B.; Li, B.; Fan, J.-X.; Zeng, X.; Zhang, X.-Z. Fluorescence light-up AIE probe for monitoring cellular alkaline phosphatase activity and detecting osteogenic differentiation. *J. Mater. Chem. B* **2016**, *4*, 4534−4541.

(53) Lim, E. K.; Keem, J. O.; Yun, H. S.; Jung, J.; Chung, B. H. Smart nanoprobes for the detection of alkaline phosphatase activity during osteoblast differentiation. *Chem. Commun.* **2015**, *51*, 3270−3272.

(54) Pittenger, M. F.; Mackay, A. M.; Beck, S. C.; Jaiswal, R. K.; Douglas, R.; Mosca, J. D.; Moorman, M. A.; Simonetti, D. W.; Craig, S.; Marshak, D. R. Multilineage Potential of Adult Human Mesenchymal Stem Cells. *Science* **1999**, *284* (5411), 143−147.

(55) Zujur, D.; Kanke, K.; Lichtler, A. C.; Hojo, H.; Chung, U.-i.; Ohba, S. Three-dimensional system enabling the maintenance and directed differentiation of pluripotent stem cells under defined conditions. *Sci. Adv.* **2017**, *3* (5), e1602875.

(56) Mostafalu, P.; Akbari, M.; Alberti, K. A.; Xu, Q.; Khademhosseini, A.; Sonkusale, S. R. A toolkit of thread-based microfluidics, sensors, and electronics for 3D tissue embedding for medical diagnostics. *Microsyst. Nanoeng.* **2016**, *2*, 16039.